e-ISSN: 2146 - 9067

**International Journal of Automotive Engineering and Technologies**

journal homepage:
https://dergipark.org.tr/en/pub/ijaet

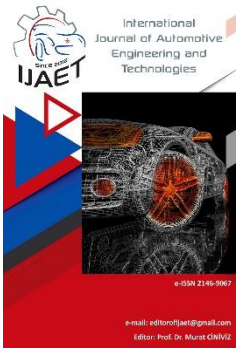


Original Research Article

# A novel design of heating system using phase change material for passenger car cabin in cold starting conditions

Habib Gürbüz[1, *], Durukan Ateş[2], Hüsameddin Akçay[3]

[1, *, 3] Department of Automotive Engineering, Faculty of Engineering, Süleyman Demirel University, Isparta, Türkiye.
[2] Graduate School of Natural and Applied Sciences, Süleyman Demirel University, Isparta, Türkiye.

**ARTICLE INFO**

Orcid Numbers
1. 0000-0001-5157-6227
2. 0000-0002-6604-7384
3. 0000-0002-5704-670X

Doi: 10.18245/ijaet.1273428

* Corresponding author
habibgurbuz@sdu.edu.tr

Received: Mar 29, 2023
Accepted: Aug 31, 2023

Published: 30 Sep 2023

Published by Editorial Board Members of IJAET

© This article is distributed by Turk Journal Park System under the CC 4.0 terms and conditions.

**ABSTRACT**

In this paper, the use of exhaust waste heat energy stored in a latent heat thermal energy storage (LHTES) system for cabin heating of a passenger car at cold climate conditions was investigated by experimental and computational fluid dynamics (CFD). A liquid circulation system was installed for this purpose, consisting of two heat exchangers, one in the passenger car's rear compartment and the other in which the phase change material (PCM) in the LHTES system was stored. Commercial RT55 paraffin wax was used as PCM, and tap water was used as heat transfer fluid (HTF). Experimental and CFD analysis studies, which started at 283 K cabin interior temperature, were continued for 1500 sec (25 min). Before the experiments, the cabin interior of the passenger car was cooled up to 283 K with the air conditioning system, and the air conditioning system was kept on at a setting where the cabin interior temperature would remain constant at 283 K during the experiments. Thus, real cold climate conditions were provided for the experimental study. As a result, it has been observed that with the new cabin heating system, thermal comfort conditions for people are provided after the first five minutes, and this temperature can be maintained throughout the experiment. So much so that the cabin temperature increased from 283 K to 295 K in five minutes and reached approximately 297 K at the end of the experiment with a slow rate of increase. Furthermore, the difference in RT55 temperatures between the experimental and CFD analysis results is less than 3% during the cabin interior heating period.

**Keywords:** Exhaust waste heat energy; LHTES; PCM; Cabin interior heating.

## 1. Introduction

It is estimated that energy consumption in the world will increase by roughly 30% in the next ten years. Researchers are therefore concerned about the issues that will arise with regard to the global economy, environment, energy security, and sustainability [1]. Internal combustion engines (ICEs), which account for a significant portion of today's fuel use, generate a lot of waste heat energy when generating energy [2]. It is crucial to develop conversion systems that take into account the intended use of the energy in order to recover the lost thermal energy in ICEs [3]. In this respect, the storage of waste energy in used systems in the energy industry comes to the fore [4]. Thermal energy storage is

an advantageous application, as the stored energy has a high potential to be converted into usable energy later [5]. Thermal energy storage systems are divided into three categories: latent heat thermal energy storage systems (LHTES), sensible heat thermal energy storage systems (SHTES), and chemical energy storage systems (CESS). Compared to SHTES, LHTES systems allow more energy to be stored per unit mass [6]. The energy stored in LHTES can be used for space heating and air conditioning systems in the automobile and building industries [7]. With LHTES systems, a large amount of thermal energy can be stored in a small container with minimum temperature change [8]. One of the new and efficient ways to store energy in my LHTES systems is to use phase change materials (PCMs). PCMs are materials that release latent heat energy during solid-to-liquid conversion or vice versa, and they store or discharge heat at an almost constant temperature [9]. Compared to other PCMs, paraffin has very high heat storage capacities. In addition, paraffins with different properties can be mixed or gradually brought together for the desired temperature ranges where the phase change will occur [10]. On the other hand, efficient thermal management in automobiles necessitates the development of novel and cutting-edge technologies and techniques designed to lower heat generation and displacement inside and around the vehicle. Because heating, ventilation, and air conditioning (HVAC) systems in cars place a significant power demand on the battery and engine, this can result in decreased fuel efficiency [11]. Therefore, it becomes crucial to provide thermal management and comfort in automobiles and to achieve this with PCM-based LHTES, which stand out in terms of making waste heat usable when their distinctive qualities are taken into account. In other words, it has been determined by the researchers that the use of PCMs, which are known to be effective in heat storage, for heat management in automobiles increases the thermal efficiency of the vehicle and improves fuel efficiency by regulating the cabin temperature [12]. It takes a certain period of time to provide thermal comfort in the cabin interior with conventional heating systems in the winter, and the fuel consumption increases as the seat heating systems used as a solution cause extra energy consumption. Therefore, besides improving engine performance, LHTES is a promising method that can control the fluctuation of the temperature profile in the cabin interior in both summer and winter months [13]. However, the design of the LHTES system to be used in an automobile is of great importance [14].

In a typical LHTES system, HTF is circulated through metal pipes to transfer heat to the PCM tank. The heat transfer fluid circulating between the inlet and outlet zones in the PCM tank creates a temperature profile. The heat transfer rate is a function of the temperature difference between the heat transfer fluid and the PCM. For this reason, the heat transfer rate of the HTF in the exit regions of the tank gradually decreases [15]. In PCMs, the time taken to melt is shorter than the solidification time. because the melting process takes place through natural convection. When a temperature gradient occurs in the liquid PCM, natural convection occurs in the liquid-solid regions. During solidification, the heat stored in the PCM is discharged out of the tank by solid conduction [16–18]. Conduction is an effective mode of solidification, and while natural convection occurs only at the beginning of solidification, after a certain period of time, natural convection loses its effect compared to conduction [19]. Many experimental and numerical studies have been carried out to investigate the thermal behavior of LHTES during melting and solidification processes [20]. Mahdi et al. [21] numerically investigated the effects of alumina nanoparticles on the solidification of a PCM in a triple tube TES system. Total solidification times were estimated for all considered nanoparticle volume fractions and temperatures of the inlet HTF. The results show that $Al_2O_3$ nanoparticles with volumetric concentrations of 3–8% provide total time savings of between 8% and 20%. Vyshak and Jilani [22] numerically analyzed the effect on melting time of tanks with different geometric properties (i.e., rectangular, cylindrical, and cylindrical shell tanks) for the LHTES system with the same volume and heat transfer surface area. The results showed that the cylindrical containers took the least time to store an equal amount of energy, and this geometric effect was more pronounced with the increase in the mass of the PCM. It was determined that as the mass of PCM filling the containers increased

from 0.24 kg to 10.69 kg, the total melting times corresponding to cylindrical and rectangular containers decreased proportionally from 0.91% to 0.54%. Thippeswmay et al. [23] experimentally investigated the charge and discharge behavior of the commercial paraffin wax used by designing a TES to store energy from hot air. An automobile radiator was placed as a heat exchanger in 11.3 kg of PCM in a glass container, and the hot air was passed through the microchannels of the heat exchanger. It has been determined that there is a temperature difference of 40–50 °C between the inlet and outlet air temperatures of the heat exchanger. During the discharge process, which lasted for 110 minutes, the outlet temperature was a maximum of 13.5 °C above the inlet air temperature. Mosaffa et al. [24] developed an approximate analytical 2D model for the solidification process of a PCM (calcium chloride hexahydrate) used for thermal storage in cylindrical and rectangular tanks with the same volume and heat transfer surface area. The thermal storage system has a height of 10 cm, a radius of 10 mm, and a cell volume of 50.3 cm3. In the analysis results, it was determined that solidification occurred approximately 10% faster in the cylindrical tank than in the rectangular one, for a 40% solidification time in PCM. Krishnamoorthi et al. [25] performed an experimental study for controlling the temperature in the cabin interior by storing the energy of the sun's rays reflected on the roof of an automobile on the PCM. A 35 x 70 x 37 cm container containing commercial paraffin wax was placed on the roof of the vehicle. In addition, a copper serpentine pipe with a diameter of 5 mm, through which the circulation water passes with the help of a 16-watt pump, and a condenser for heat discharge are placed. The experiments were carried out between 10:00 and 15:00. In the experiments conducted for three different experimental groups in which only PCM, water circulation without PCM, or both PCM and water circulation were provided, cabin temperatures were compared. As a result, it has been determined that it can be reached at 36 °C, which is the closest to the atmospheric temperature, in 11 minutes with PCM-coated copper tubing. Gübrüz et al. [26] experimentally investigated the solidification process of the LHTES system, in which the heat energy thrown into the atmosphere along with the exhaust gases from the internal combustion vehicles is stored by the PCM. In the LHTES system, RT55 paraffin wax enriched with $Al_2O_3$ nanoparticles was used as PCM. The heat energy stored in the LHTES was discharged into the cabin interior by the heating radiator through the closed-circuit liquid circulation system. Experimental studies under real climatic conditions were performed only for RT55 and five different $Al_2O_3$ fractions (5% weight, 10% weight, 15% weight, 20% weight, and 25% weight). The experiments were carried out for 1200 seconds. As a result, it was determined that increasing the $Al_2O_3$ fraction by up to 10% improved the solidification process and increased the cabinet temperature by about 29% compared to using pure RT55.

Considering the literature, there are a limited number of experimental and numerical analysis studies on the use of exhaust waste heat energy stored in the LHTES system for cabin interior heating, although it is a good alternative. In addition, previous studies of in-vehicle heat management generally used an external heat source (such as solar energy) to store heat in the PCM instead of waste heat from the ICE. For this reason, it is considered that ICE's waste heat energy is not adequately addressed in terms of providing in-vehicle thermal comfort. In this respect, some of the prominent aspects of this study are as follows:

- Developing an inexpensive and highly accessible PCM-containing LHTES system in order to provide cabin interior thermal comfort in a passenger car,
- Using only ICE's own waste heat energy, without the need for an additional external source, in order to provide thermal comfort in the passenger car cabin interior,
- Ensuring cabin interior thermal comfort in a relatively shorter time and without using additional fuel energy with the heat energy stored in the PCM, especially during the first cold start conditions in the winter months.

Finally, in this paper, the use of exhaust waste heat energy stored in the LHTES system for cabin heating of a passenger car in winter was investigated by experimental and CFD analysis. Experimental and CFD analysis studies, which started at a 283 K interior temperature, continued for 1500 seconds (25 minutes). The cabin temperature rose from 283 K to 295 K in

five minutes and reached approximately 297 K at the end of the experiment with a slow increase. In addition, it was determined that the RT55 temperature difference between the experimental and CFD analysis results was less than 3% during the cabin heating period.

## 2. Material and Methods

### 2.1. Design of cabin interior heating system with LHTES (experimental setup)

The experimental study was performed in a typical 5-seat passenger car with a heating area of 2.88 $m^3$ (including cargo volume). A tubular finned heater core and blower motor with dimensions of 154 (W) x 193.5 (L) x 26 (H) mm are placed between the rear seats of the passenger car to allow air flow in the cabin interior. Before the experiment, the air conditioning system was operated for approximately 45 minutes under the idling conditions of the passenger car engine until the temperature in the cabin interior reached 283 K. Then, the air conditioner system was adjusted so that the cabin interior temperature remained constant at 283 K. Thus, real-world cold climate conditions were provided during the experiment. In order to store the RT55 in the LHTES system, a steel-bodied cylindrical tank with a diameter of 23 cm and a height of 21 cm, with outer surfaces covered with glass wool and aluminum foil, was used. In order to transfer the heat from the RT55 in the liquid phase to the HTF, a two-layer, coil-type heat exchanger inside the cylindrical tank is designed. The outer layer is produced from a copper tube with an outer diameter of 10 mm, a coil diameter of 150 mm, a length of 150 mm, and 8 helices. The inner layer is produced from a copper tube with an outer diameter of 9 mm, a coil diameter of 75 mm, a length of 150 mm, and 16 helices. RT55 used as PCM has a latent heat of fusion of 170 kJ/kg, a specific heat of 2 kJ/kgK, a density of 880/770 (solid/liquid) kg/$m^3$, a thermal conductivity of 0.2 W/mK, a solidification temperature of 324 K, and a maximum operating temperature of 90 °C [27]. The temperature of the RT55 in the tank was measured by two pieces of K-type probe thermocouples from its center ($T_{PCM\_center}$) and side ($T_{PCM\_side}$). Before the experiments, the RT55 in the LHTES tank was in the liquid phase at a temperature of 353 K. The connection between the heater core and the coil-type heat exchanger is provided by a coolant hose with an inner diameter of 9 mm, and the outer surfaces are covered with glass wool and aluminum foil. A 4.2 W DC liquid pump was used for the circulation of the HTF. The liquid pump was operated at half load, and the flow rate of the HTF was adjusted to 2 l/min. The inlet ($T_{PCM\_water\_in}$) and outlet ($T_{PCM\_water\_out}$) temperatures of the HTF from the LTES tank were measured by two pieces of K-type probe thermocouples. In addition, passenger car interior temperature was measured from the middle point of the interior volume with a K-type probe thermocouple. The temperatures measured at 1-second intervals were collected on the computer via a data acquisition card. The experimental layout of the cabin interior heating system with LHTES is given in Fig.1.

### 2.2. CFD analysis procedure and governing equations

For CFD analysis, 3D models were created using LHTES tank and coil-type heat exchanger measurements used in the experimental cabin interior heating system. A tetrahedral mesh geometry consisting of a “Skewness value” of 0.9054, a “Node value” of 597.324, and 2.883.601 “Elements” was created in the LHTES tank. In CFD analysis, the inlet and outlet of tap water to the LHTES tank for the heat discharge process were defined as "inlet" and "outlet", respectively.

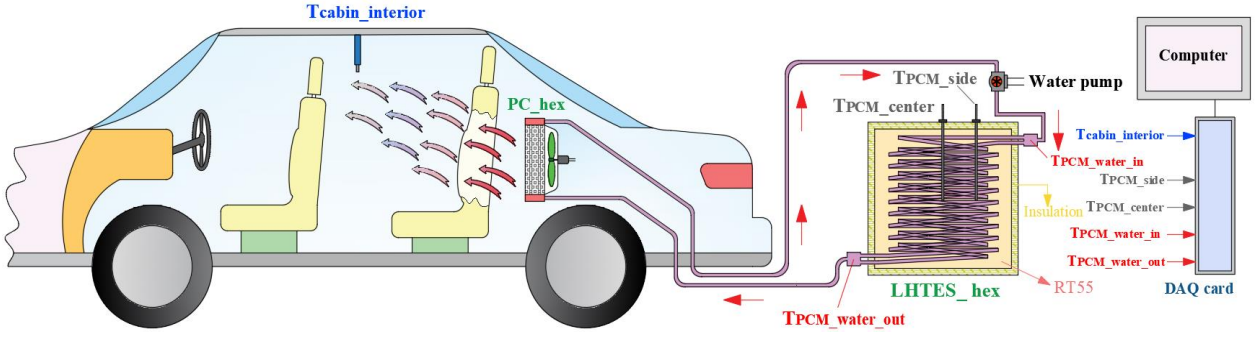


Fig.1. Experimental layout of cabin interior heating system with LHTES.

In addition, the surface of a coil-type heat exchanger and PC_hex is defined as "wall". While preparing the 3D model for the cooling process, the initial limit values were 283.15 K for HTF, 353.15 K for FDM, and 283.15 K for the heat exchanger “wall” surface, and analyses were performed with the assumption that there is no heat transfer from other surfaces. Throughout the CFD analysis, the calculation steps were continued with the average surface temperature values taken over both PC_hex and LHTES_hex surfaces. The 3D model and mesh structure of the LHTES tank and coil-type heat exchanger are given in Fig.2.

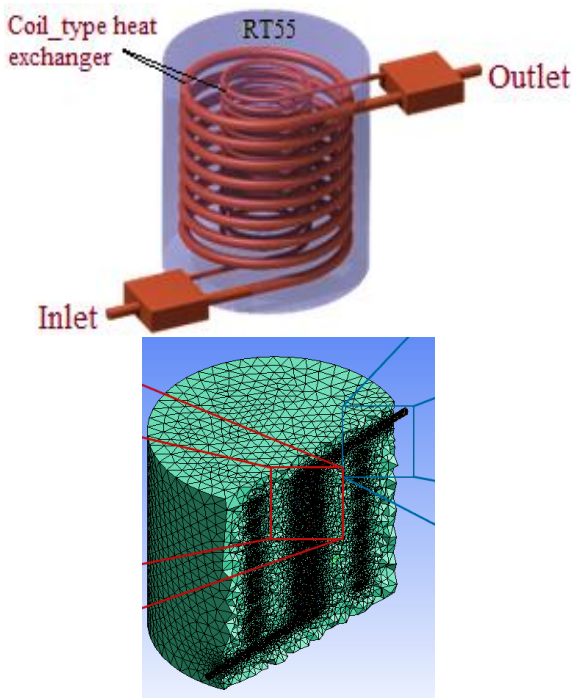


Fig.2. 3D model and mesh structure of the LHTES tank and coil-type heat exchanger

A user-define-functions code was created in order to advance the closed-circuit tap water circulation steps. In the first step of the code, the calculation is made with the initial limit values, and the average surface temperature values at the outputs of LHTES_hex and PC_hex are recorded. In the next step, the output average surface temperature of PC_hex is added to the input average surface temperature of the LHTES tank, and the output average surface temperature of the LHTES tank is added to the input average surface temperature of PC_hex. This closed-loop calculation process continues step by step until the CFD analysis is complete. The CFD analysis was performed using the turbulent flow model (RNG k-ε) as time-dependent by ANSYS Fluent 14.5 software. The governing equations used are defined in equations 1–12 [28]. The film sub-time steps used to advance the film time to the same physical flow are solved with Eq.1(transient equation).

$$\Delta t = \frac{\Delta t_{flow}}{N_{film}} \quad (1)$$

Where $\Delta t_{flow}$ and $N_{film}$ represent steps of the flow time and the number of film times, respectively. The general Continuity equation (Eg.2) and Momentum equation (Eq.3) were used for the progress steps of the CFD analysis as follows:

$$\frac{\partial \rho}{\partial t} + \nabla \cdot (\rho\, \vec{v}) = S_m \quad (2)$$

$$\frac{\partial}{\partial t}(\rho\vec{v}) + \nabla \cdot (\rho\vec{v}\vec{v}) = -\nabla p + \nabla(\bar{\bar{\tau}}) + \rho\vec{g} + \vec{F} \quad (3)$$

Where $S_m$, $\rho$, and $\vec{v}$ represents the mass that transferred between phases in the two-phase case, the density, and the velocity vector, respectively. In Eq.3, $p$, $\rho\vec{g}$, $\vec{F}$ and $\bar{\bar{\tau}}$ represent the static pressure, the gravity body force, the outer body forces, and the stress tensor (Eq.4), respectively.

$$\bar{\bar{\tau}} = \mu\left[(\nabla\vec{v} + \nabla\vec{v}^T) - \frac{2}{3}\nabla \cdot \vec{v} I\right] \quad (4)$$

Where $\mu$ and $I$ represent the molecular viscosity and the unit tensor, respectively. In the solidification process, the modified momentum equation (Eq.5) is used to take into account the porosity structure in the mushy region.

$$S = \frac{(1-\beta)^2}{(\beta^3+\varepsilon)} A_{mush}\left(\vec{v} - \overrightarrow{v_p}\right) \quad (5)$$

Where β, $\varepsilon$, $A_{mush}$, $\vec{v}$ and $\overrightarrow{v_p}$ represent the liquid fraction, the number for divide-by-zero error, the mushy region constant ($10^{-6}$), and the shrinkage velocities, respectively. In the CFD analysis, the energy change is calculated using Eq.6 (the energy equation).

$$\frac{\partial}{\partial t}(\rho E) + \nabla \cdot \left(\vec{v}(\rho E + p)\right) = \nabla \cdot \left(k_{eff}\nabla T - \sum_j h_j \vec{J}_j + \left(\bar{\bar{\tau}}_{eff} \cdot \vec{v}\right)\right) + S_h \quad (6)$$

Where $E$, $k_{eff}$, $\vec{J}_j$, $h_j$ and $S_h$ define the total energy, the heat transfer coefficient, the diffusion flux, the enthalpy, and the heat generated by any method, respectively. The total enthalpy (or heat content) is calculated as the

sum of the sensible (ΔH) and latent heats (h) by Eq.7.

$$h = h_{ref} + \int_{T_{ref}}^{T} c_p dT \quad (7)$$

Where $h_{ref}$, $T_{ref}$, and $c_p$ are the reference enthalpy, temperature, and specific heat, respectively. The liquid fraction is determined depending on the temperature, as in Eq.8.

If $\beta = 0$ then $T < T_{solidus}$

If $\beta = 1$ then $T < T_{liquidus}$

If $\beta = \frac{T - T_{solidus}}{T_{liquidus} - T_{solidus}}$ then $T_{solidus} < T < T_{liquidus}$ (8)

Where $T_{solidus}$ and $T_{liquidus}$ are the solidification and liquefaction temperatures, respectively. In order to take into account, the latent heat energy generated during the phase change, the modified version of Eq.6, Eq.9 is used.

$$\frac{\partial}{\partial t}(\rho H) + \nabla \cdot (\rho \vec{v} H) = \nabla \cdot (k \nabla T) + S \quad (9)$$

Where *k* represents the heat transfer coefficient. Eq.5 is modified as in Eq.10 to calculate turbulence in mush and solidification regions depending on the liquid fraction during solidification.

$$S = \frac{(1-\beta)^2}{(\beta^3 + \varepsilon)} A_{mush} \emptyset \quad (10)$$

Where $\emptyset$ represents the amount of turbulence dissolved. The transport equations of the RNG k-ε model used for turbulent flow are as in Eq.11 and Eq.12.

$$\frac{\partial}{\partial t}(\rho k) + \frac{\partial}{\partial x_i}(\rho k u_i) = \frac{\partial}{\partial x_j}\left(\alpha_k \mu_{eff} \frac{\partial k}{\partial x_j}\right) + G_k + G_b - \rho\varepsilon - Y_M + S_k \quad (11)$$

$$\frac{\partial}{\partial t}(\rho \varepsilon) + \frac{\partial}{\partial x_i}(\rho \varepsilon u_i) = \frac{\partial}{\partial x_j}\left(\alpha_\varepsilon \mu_{eff} \frac{\partial \varepsilon}{\partial x_j}\right) + C_{1\varepsilon}\frac{\varepsilon}{k_e}(G_k + C_{3\varepsilon} G_b) - C_{2\varepsilon}\rho\frac{\varepsilon^2}{k_e} - R_\varepsilon + S_\varepsilon \quad (12)$$

Where $G_k$ is the generation of turbulent kinetic energy with the effect of an average velocity gradient, and $G_b$ is the generation of turbulent kinetic energy with the effect of buoyancy. $Y_M$ represents the effect of unstable compressible turbulence on the total dispersion rate. $\alpha_k$ and $\alpha_\varepsilon$ are inverse Prandtl numbers for $k_e$, and, $\varepsilon$, while $S_k$ and $S_\varepsilon$ are user-defined numbers. $k_e$, $\varepsilon$, $\mu_{eff}$, $u$ and $R_\varepsilon$ represent kinetic energy per mass, turbulence dispersion ratio, effective dynamic viscosity, velocity vector, and gas constant, respectively. The values of the model constants, $C_{1\varepsilon}$ and $C_{2\varepsilon}$, are 1.44 and 1.68, respectively. The analysis algorithms used in CFD analysis is given in Table 1.

Table 1. Analysis algorithms used in CFD analysis

| Schemes | Analysis algorithms |
|---|---|
| Pressure-Velocity Coupling | SIMPLE |
| Pressure | PRESTO! |
| Momentum | Second Order Upwind |
| Energy | Second Order Upwind |
| Transient Formulation | First Order Implicit |

### 2.3. Calculation of stored energy in LHTES

The total heat energy recovered by the heat discharge from the liquid RT55 in the LHTES tank is calculated by Eq.13.

$$\dot{E}_{total} = \dot{E}_{s\_phase} + \dot{E}_{l\_phase} + \dot{E}_{l\_heat} \quad (13)$$

Where $\dot{E}_{l\_heat}$ is energy released as latent heat during solidification process, $\dot{E}_{l\_phase}$ is the energy of the liquid RT55, and $\dot{E}_{s\_phase}$ is the energy of the solid RT55. These are calculated with the following equations:

$$\dot{E}_{l\_heat} = m_{RT55} * L_{fr} * L_{f\_heat} \quad (14)$$

$$\dot{E}_{l\_phase} = \dot{m}_{l\_phase} * cp_{l\_phase} * \Delta T_{l\_phase} \quad (15)$$

$$\dot{E}_{s\_phase} = \dot{m}_{s\_phase} * cp_{s\_phase} * \Delta T_{s\_phase} \quad (16)$$

Where $m_{RT55}$ is the total mass of RT55 (kg), $L_{fr}$ is the liquid fraction during heat discharge (%), $L_{f\_heat}$ is the latent heat of fusion of RT55 (kJ/kg), $\dot{m}_{l\_phase}$ is the instantaneous mass of liquid RT55 (kg), $\dot{m}_{s\_phase}$ is the instantaneous mass of solid RT55 (kg), $cp_{l\_phase}$ and $cp_{s\_phase}$ are the specific heats for liquid and solid RT55 (kJ/kgK), $\Delta T_{l\_phase}$ and $\Delta T_{s\_phase}$ are the temperature differences of liquid and solid RT55 (K).

## 3. Results and Discussion

Fig.3 shows the variation of the LHTES system and cabin interior temperatures during cabin heating (experimental). Before the experiments, the RT55 in the LHTES tank was in the liquid phase at a temperature of 353 K, while the interior temperature of the passenger car and the temperature of the HTF were approximately 283 K. With the start of the experiments, the inlet and outlet temperatures of the LHTES tank of

the HTF decreased rapidly; the inlet temperature ($T_{PCM\_water\_in}$) decreased to approximately 320 K after 150 seconds, and the outlet temperature ($T_{PCM\_water\_out}$) decreased to approximately 329 K after 90 seconds. The inlet temperature of the HTF circulating in the heat exchanger in the cabin for heating purposes into the LHTES tank reached its maximum value later than the outlet temperature. Then, both temperatures started to decrease again, synchronized with each other towards the end of the experiment, and equalized at approximately 308 K. Similar to the inlet and outlet temperatures of the HTF, the temperature in the center and side of the RT55 in the LHTES tank decreased rapidly within the first 45 seconds, decreasing to 338 K in the center ($T_{PCM\_center}$) and 329 K at the side ($T_{PCM\_side}$). In contrast, the PCM_side temperature decreased to about 321 K at the end of the experiment, while the PCM_center temperature decreased to approximately 313 K at the end of the experiment. This finding indicates that solidification in the RT55 during the cabin interior heating period is greater at the center of the LHTES tank than at its sides. In addition, the temperature of the RT55 in the center of the LHTES tank is very close to the temperature of the HTF circulated in the coil-type heat exchanger of the LHTES tank. In fact, the 5 K temperature difference between HTF ($T_{PCM\_water\_in}$ and $T_{PCM\_water\_out}$) and $T_{PCM\_center}$ indicates that there is still heat that can be transferred to the cabin air from the LHTES system. The cabin interior temperature, which was 283 K at the beginning of the experiments and kept constant by the air conditioning system, increased rapidly within the first 5 minutes and reached 295 K. The cabin interior temperature, which was 283 K at the beginning of the experiments and kept constant by the air conditioning system, increased rapidly within the first 300 seconds (5 minutes) and reached 295 K. In fact, at the very beginning of the experiment, there is a short period (the first 30 seconds) during which the interior temperature has a very low rate of rise. The temperature, which reached 295 K in the first 5 minutes, maintained this value until the end of the experiment and even increased to 297 K at the end of the experiment. Considering the 5 K difference between the center temperature of the RT55 and the temperature of the HTF at the end of the experiment, it is also seen that the cabin temperature can be maintained at 297 K for a longer period of time with the LHTES system. The results are in agreement with previous studies. In a paper on in-cabin heating with the LHTES system using the RT55 as the PCM, the temperature in the center of the PCM dropped from 366 K to 350 K after 1200 seconds. The temperature inside the cabin, which was 275 K at the beginning, increased to 279 K after 1200 seconds, and the cabin interior temperature increased by approximately 4.2 °C [26].

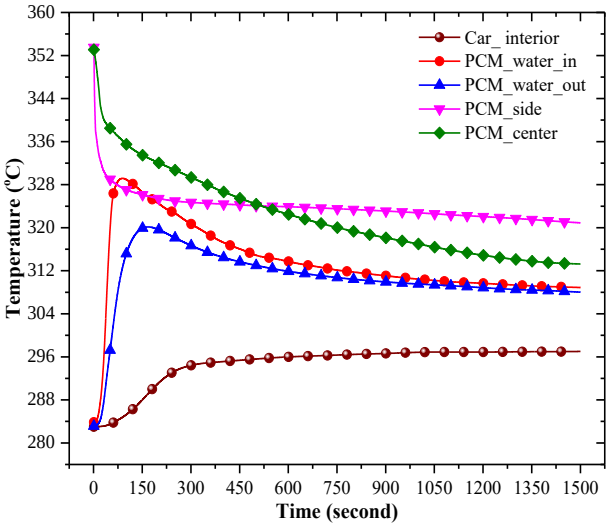


Fig. 3. Variation of the LHTES system and cabin interior temperatures during cabin heating (experimental)

In Fig.4(a), the variation of RT55 temperature with time according to the experimental and CFD analysis results during the cabin interior heating period is given, and the difference between the experimental and CFD temperature results of RT55 is given in Fig.4(b). As seen in Fig.4(a), the experimental side temperature of the RT55 and the average RT55 temperature curves of the CFD analysis have a very similar profile and numerical values over the cabin interior heating period. However, the experimental RT55 center temperature has a different curve and numerical values than the average RT55 temperature of the CFD analysis. Despite that, the difference between both the experimental RT55 side temperature and the experimental RT55 center temperature and the average RT55 temperature of the CFD analysis is less than 3% over the entire cabin interior heating period [see Fig.4(b)].

Fig.5 illustrates the variation of temperature contours during the heat discharge process. The temperature decrease, which occurs with the

start of the heat discharge in the RT55, which is initially at 353 K inside the LHTES tank, first starts around the coil-type heat exchanger and proceeds from the bottom of the tank to the upper surface (up to 200 seconds). After the 200th second, the RT55 temperature, which was in the range of 322–330 K in the entire volume of the LHTES tank (except for around the coil type heat exchanger), remained almost unchanged in this range until the end of the experiment. A temperature gradient in the range of 283–300 K occurs around the serpentine-type heat exchanger, and it is seen that this region expands continuously until the end of the experiment. In these regions, the temperatures decreased well below the solidification temperature of the RT55 (324 K).

The variation of the RT55 average temperature during the heat discharge is given in Fig.6(a), and the variation of the heat flux is given in Fig.6(b). The average temperature of the RT55, which was 353 K at the beginning, decreased rapidly to 329 K up to the 200th second and then reached 322 K at the end of the analysis with a slowing rate of decrease. The heat flux, which reached its maximum value approximately 30 seconds after the start of the heat discharge, decreased rapidly up to the 450th second, and then the rate of decrease in the heat flux progressed very slowly until the end of the heat discharge.

Fig.7 shows the variation in the liquid fraction contours during the heat discharge process. At the beginning of the CFD analysis, in the RT55, which was completely in the liquid phase inside the LHTES tank, the solidification that started

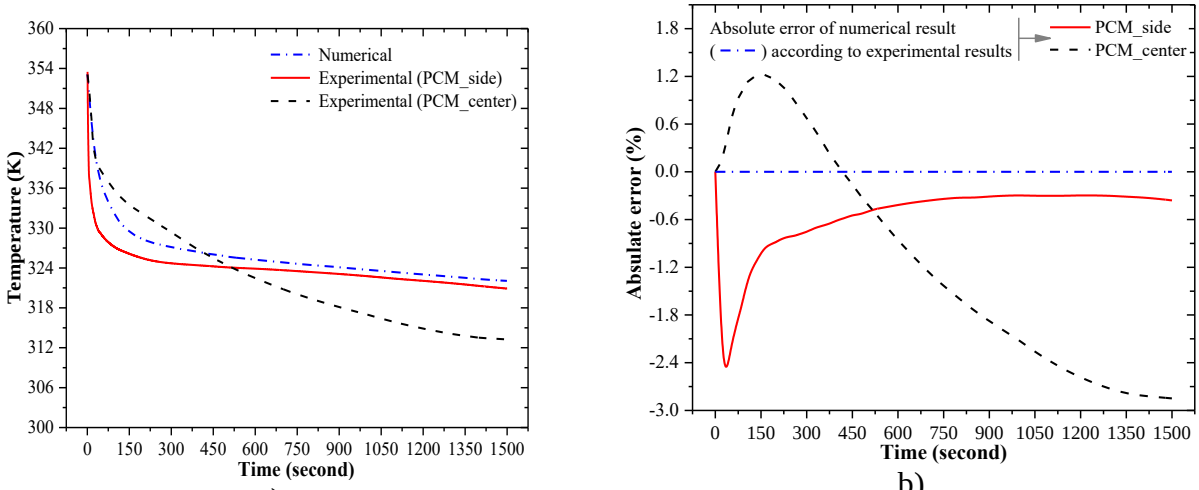


a) b)

Fig.4(a) Variation of experimental and CFD temperature results of RT55 during the cabin interior heating period, and (b) the difference between the experimental and CFD analysis temperature results of RT55

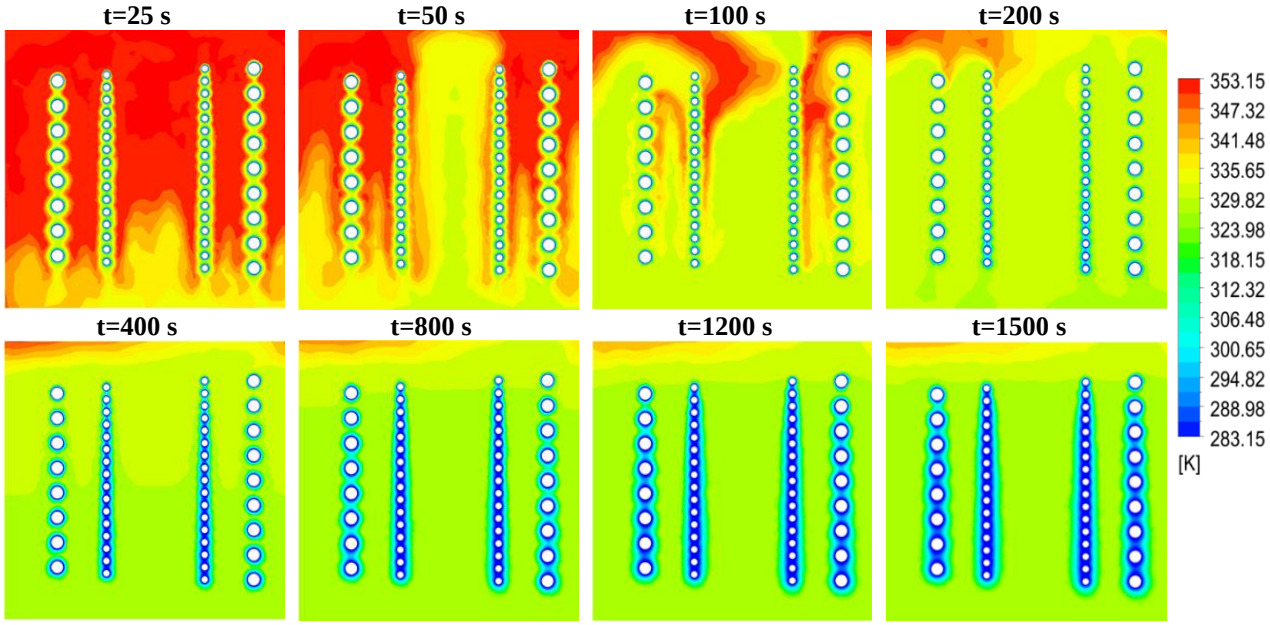


Fig.5. Variation of temperature contours during heat discharge process

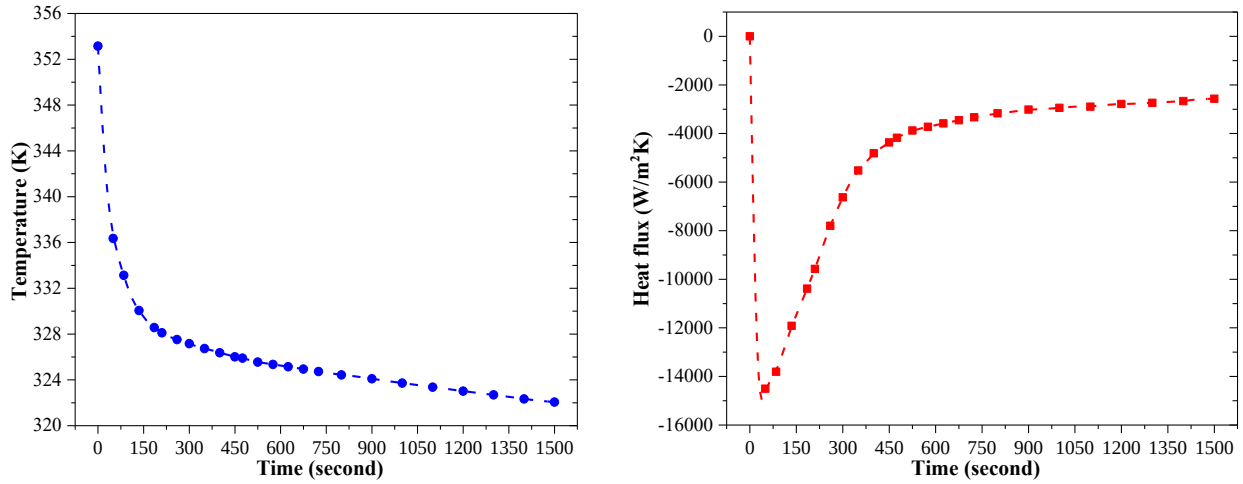


a) b)

Fig.6 (a) Variation of average temperature of RT55, and (b) heat flux during the heat discharge process

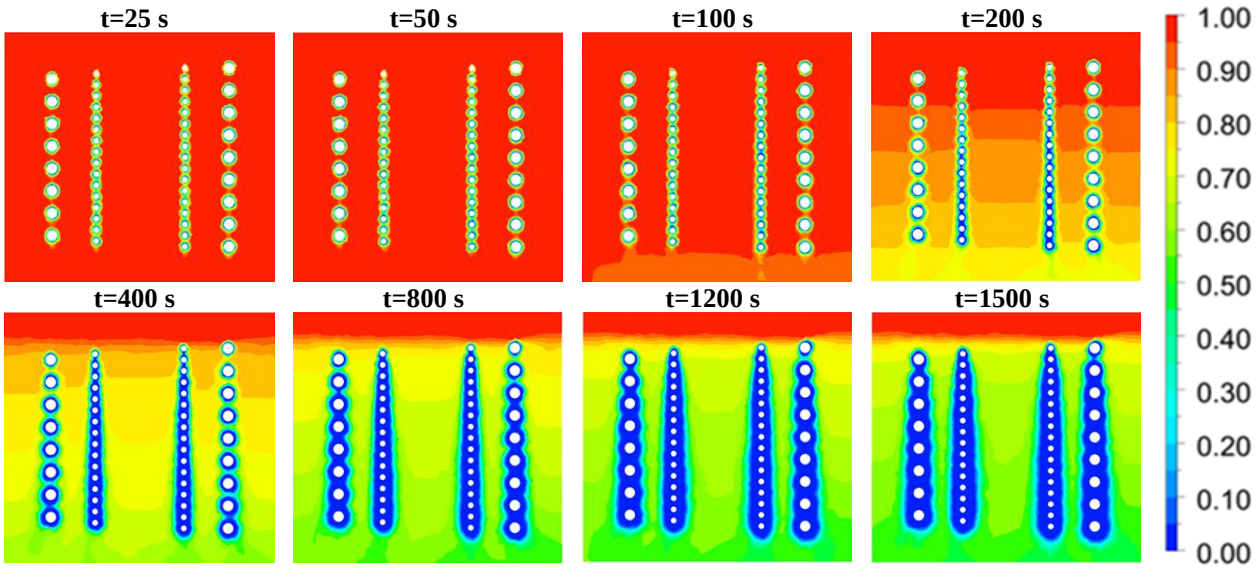


Fig.7. Variation of liquid fraction contours during the heat discharge process

around the coil type heat exchanger with the heat discharge first spread towards the bottom of the tank and then proceeded towards to the upper surface. However, even at the end of the experiment, it is seen that the RT55 in a thin layer at the top of the coil type heat exchanger still has not solidified. On the other hand, the full solidification process that started around the coil-type heat exchanger after 200 seconds increased rapidly and became a remarkable layer at the end of the experiment. This finding shows that the solidification in the RT55 inside the LHTES tank starts around the coil-type heat exchanger and spreads to the remaining volume. The variation of the average liquid fraction during the heat discharge process is given in Fig.8(a), and the released heat energy from RT55 during cabin interior heating (heat discharge) is given in Fig.8(b). At the beginning of the CFD analysis, the liquid RT55 inside the LHTES tank has a solidification process that slows down from the beginning to the end of the experiment with heat release. The solidification process, which slowed significantly near the end of the experiment, resulted in a 46% liquid fraction. The main reason for this is the decrease in the heat transfer rate due to the increase in the temperature of the heating volume, which has a temperature of 283 K at the beginning, and the decrease in the heat energy stored in the LHTES tank over time. As seen in Fig.8(b), with the start of the heat discharge process, the amount of heat transferred from the liquid RT55 in the LHTES tank to the HTF increased, and the total amount of heat released from the RT55 reached 1141 kJ at the 1500th second. At the beginning of the heat release process, the amount of heat released as latent heat with heat discharge in RT55, which was completely in the liquid phase at the beginning of the experiment, and the amount of

sensible heat released from the solid phase of RT55 increased, while the amount of sensible heat released from the liquid phase of RT55 decreased.

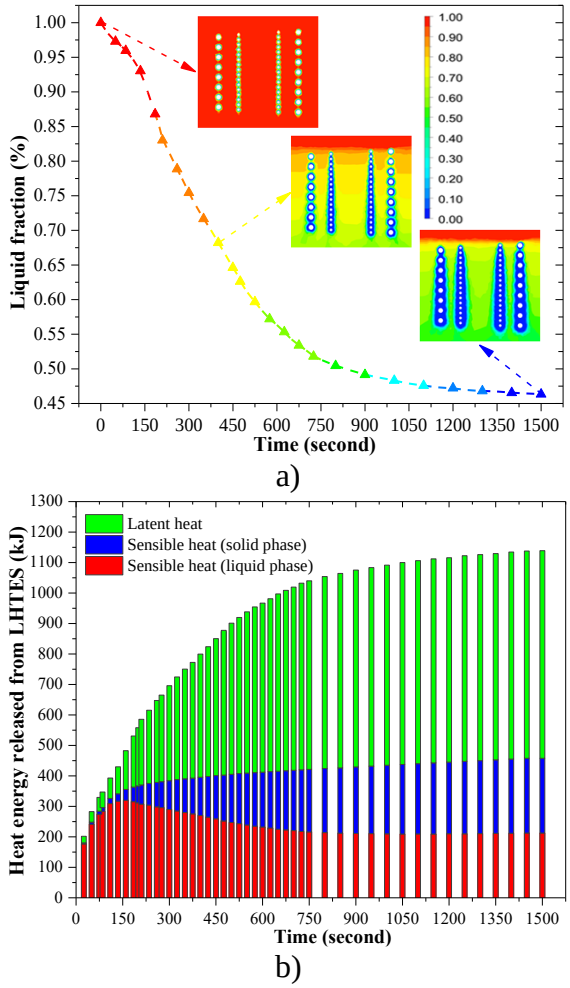


Fig.8(a) Variation of average liquid fraction, and (b) released heat energy from RT55 during heat discharge process

Fig.9 illustrates the variation of flow speed contours during the heat discharge process. With the start of the heat release, the flow speeds of the RT55 around the coil heat exchanger decreased to 0.01 m/s, and after the 200th second, the flow movement around the coil heat exchanger came to a standstill (approximately 0 m/s) with the onset of full solidification. In fact, just outside the solidification layer in the coil-type heat exchanger body, there is also a thin layer of RT55 with flow speeds varying between 0.02-0.03 m/s (see the flow speed contour at the 100th second). In addition, it is seen that the decrease in flow speeds with solidification extends to the entire volume of the LHTES tank. It should be noted that the regions where the flow rates came to a standstill during the heat discharge correspond to the regions where full solidification takes place in the fluid fraction contours in Fig.7.

## 4. Conclusions

The general results of the study in which the use of exhaust waste heat energy stored in the LHTES system for cabin interior heating of a passenger car in cold climate conditions was examined by experimental and CFD analysis are listed as follows:

At the start of the experiment, the RT55 in the LHTES tank is in the liquid phase at a temperature of 353 K, while the interior temperature of the passenger car and the temperature of the HTF are approximately 283 K. On the other hand, the inlet and outlet temperatures of the HTF, which were 283 K at the beginning of the experiment, reached 308 K

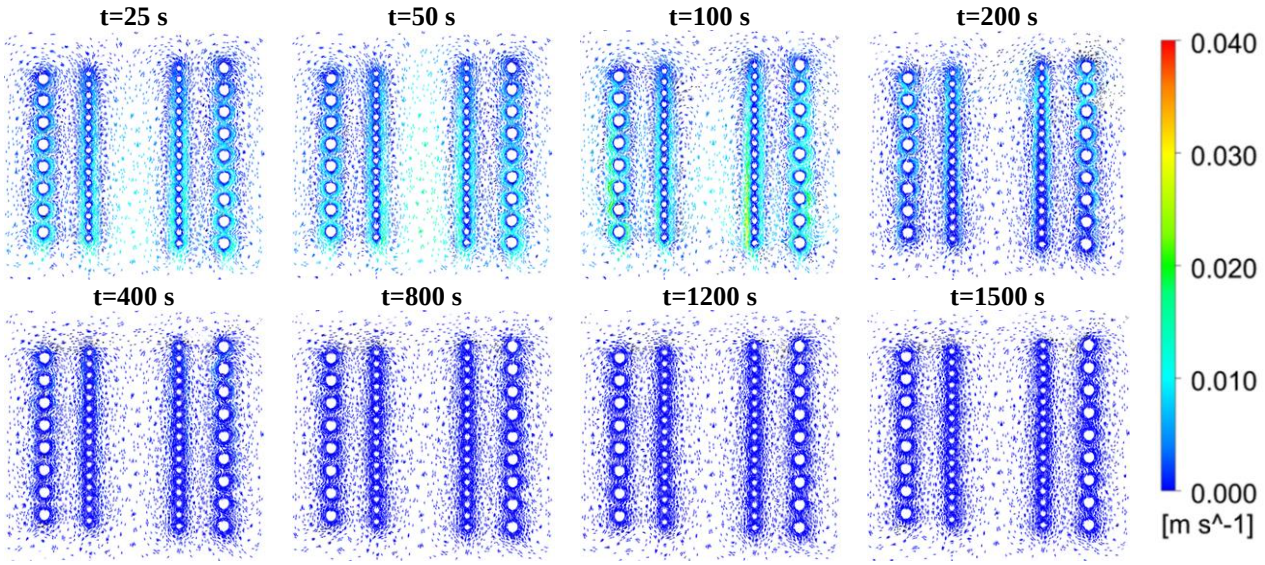


Fig.9. Variation of flow speed contours during the heat discharge process

at the end of the experiment, almost equalizing each other. The temperature of the cabin interior, which was 283 K at the beginning of the experiment, reached 295 K within the first 5 minutes with the start of the heat discharge from the LHTES system, maintained this value up to the end of the experiment, and even increased up to 297 K.

- There is less than a 3% difference between the experimental and CFD analysis temperature results of the RT55 inside the LHTES tank during cabin interior heating (heat discharge). This finding shows that the temperature, liquid fraction, and velocity contours and numerical values obtained by CFD analysis are quite close to the experimental results and are reliable.
- The CFD analysis results (i.e., temperature and liquid fraction) show that the solidification process in the RT55 inside the LHTES tank during heat discharge starts around the coil-type heat exchanger and spreads from the bottom of the tank to the upper surface. At the end of the heat discharge process, it was observed that approximately 54% of the RT55 in the LHTES tank had solidified (46% liquid fraction), and the flow speeds around the serpentine-type heat exchanger approached zero. The total heat (latent and sensible) released in 1500 seconds with the heat discharge from the RT55, which is completely in the liquid phase at the beginning, is 1141 kJ.

The general findings of the paper show that the thermal comfort of the driver and passengers via the cabin interior heating system realized with the LHTES system can be provided in as little as 5 minutes, and these conditions can be protected for more than 25 minutes. In future studies, it is important to integrate the cabin interior heating system, which has the LHTES system, with the air conditioning system of the car and test it in real-word climate conditions.

**Acknowledgment**

This article was presented as part of the M.Sc. thesis, in which was prepared by Durukan ATEŞ [29] supervised by Habib Gürbüz**.**

**CRediT authorship contribution statement**

**Habib Gürbüz**: Supervision, Materials and Method, Conceptualization, Experimental Study, Discussion, and Conclusions.

**Durukan Ateş:** Experimental Study, CFD analysis, Validation, Data collection, Materials and Method, and Results and Discussion.

**Hüsameddin Akçay:** Experimental Study, Data collection, Materials and Method, and Results and Discussion.

**Declaration of Competing Interest**

The authors declare that they have no known competing financial interests or personal relationships that could have appeared to influence the work reported in this paper

**Nomenclature**

| | |
|---|---|
| CFD | Computational fluid dynamics |
| HTF | Heat transfer fluid |
| LHTES | Latent heat thermal energy storage |
| PCM | Phase-change material |
| $\vec{v}$ | Velocity vector |
| $\dot{E}_{l\_heat}$ | Energy released as latent heat during the solidification process |
| $\dot{E}_{l\_phase}$ | Energy of the liquid RT55 |
| $\dot{E}_{s\_phase}$ | Energy of the solid RT55 |
| $\dot{E}_{total}$ | Total energy stored by RT55 |
| $\vec{J}_j$ | Diffusion flux |
| $\dot{m}_{l\_phase}$ | Instantaneous mass of liquid |
| $\dot{m}_{s\_phase}$ | Instantaneous mass of solid |
| $\overrightarrow{v_p}$ | Shrinkage velocities |
| $\bar{\bar{\tau}}$ | Stress tensor |
| $\Delta t_{flow}$ | Flow time |
| $\vec{F}$ | Outer body forces |
| $L_{f\_heat}$ | Latent heat of fusion |
| $L_{fr}$ | Liquid fraction |
| $N_{film}$ | Number of film time |
| $cp_{l\_phase}$ | Specific heats for liquid |
| $cp_{s\_phase}$ | Specific heats for solid |
| $m_{RT55}$ | Total mass of RT55 |
| $\emptyset$ | Amount of turbulence dissolved |
| $\Delta H$ | Sum of the sensible |
| $A_{mush}$ | Mushy region constant ($10^{-6}$) |
| $c_p$ | Specific heat |
| $E$ | Total energy |
| $G_b$ | Generation of turbulent kinetic energy with the effect of buoyancy |
| $G_k$ | Generation of turbulent kinetic energy with the effect of an average velocity |

gradient

| | |
|---|---|
| h | Latent heats |
| $h$ | Enthalpy |
| $k_{eff}$ | Heat transfer coefficient |
| $S_h$ | Heat generated by any method |
| $S_m$ | Mass that transferred between phases in the two-phase case |
| $T_{liquidus}$ | Liquefaction temperatures |
| $T_{ref}$ | Temperature |
| $T_{solidus}$ | Solidification temperatures |
| β | Liquid fraction |
| $\varepsilon$ | Number for divide-by-zero error |
| $M$ | Molecular viscosity |
| $\rho$ | Density |
| $I$ | Unit tensor |
| $p$ | Static pressure |
| $\rho\vec{g}$ | Gravity body force |

## 5. References


1. OGJ Editors, "BP Energy Outlook: Global energy demand to grow 30% to 2035," Oil & Gas Journal, 2017.
2. Saidur R, Rezaei M, Muzammil WK, Hassan MH, Paria S, Hasanuzzaman M. "Technologies to recover exhaust heat from internal combustion engines" Renew Sustain Energy Rev 2012;16(8):5649-5659.
3. Farhat O, Faraj J, Hachem F, Castelain C, Khaled M. "A recent review on waste heat recovery methodologies and applications: Comprehensive review, critical analysis and potential recommendations" Clean. Eng. Technol, 6, 100387, 2022.
4. Ismail KA, Lino FA, Machado PLO, Teggar M, Arıcı M, Alves TA, Teles MP, "New potential applications of phase change materials: A review", Journal of Energy Storage, 53, 105202, 2022.
5. Sharma A, Tyagi VV, Chen CR, Buddhi D, "Review on thermal energy storage with phase change materials and applications", Renewable and Sustainable energy reviews, 13(2), 318-345, 2009.
6. Krishna J, Kishore PS, Solomon AB, "Heat pipe with nano enhanced-PCM for electronic cooling application", Experimental Thermal and Fluid Science, 81, 84-92, 2017.
7. Mishra L, Sinha A, Gupta R, "Recent developments in latent heat energy storage systems using phase change materials (PCMs)-a review", Green Buildings and Sustainable Engineering: Proceedings of GBSE 2018, 25-37. 2019.
8. Kang Y, Zhang Y, Jiang Y, Zhu Y, "General Model of Analyzing the Thermal Performance of Latent Heat Thermal Energy Storage Systems with Various PCM Capsules", Energy Engineering, 788, 2000.
9. Iqbal K, Sun D, "Synthesis of nanoencapsulated Glauber's salt using PMMA shell and its application on cotton for thermoregulating effect" Cellulose, 25(3), 2103-2113, 2018.
10. Watanabe T, Kanzawa A, "Second law optimization of a latent heat storage system with PCMs having different melting points", Heat Recovery Systems and CHP, 15(7), 641-653, 1995.
11. Marshall GJ, Mahony CP, Rhodes MJ, Daniewicz SR, Tsolas N, Thompson SM. "Thermal management of vehicle cabins, external surfaces, and onboard electronics: An overview" Engineering, 5(5), 954-969, 2019.
12. Sood D, Das D, Ali SF, Rakshit D, "Numerical analysis of an automobile cabin thermal management using passive phase change material", Thermal Science and Engineering Progress, 25, 100870, 2021.
13. Jamekhorshid A, Sadrameli SM, "Application of phase change materials (PCMs) in maintaining comfort temperature inside an automobile" World Academy of Science, Engineering and Technology, International Journal of Chemical, Molecular, Nuclear, Materials and Metallurgical Engineering, 6(1), 3, 2012.
14. Gürtürk M, Kok B, "A new approach in the design of heat transfer fin for melting and solidification of PCM", International Journal of Heat and Mass Transfer, 153, 119671, 2020.
15. Aldoss TK, Rahman MM, "Comparison between the single-PCM and multi-PCM thermal energy storage design", Energy conversion and management, 83, 79-87, 2014.
16. Lamberg P, Siren K, "Approximate analytical model for solidification in a finite PCM storage with internal fins", Applied Mathematical Modelling, 27(7), 491-513, 2003.
17. Stritih U, Novak P, "Heat transfer enhancement at phase change processes", 2000.
18. Kroeger PG, Ostrach S, „The solution of a two-dimensional freezing problem including convection effects in the liquid region", International Journal of Heat and Mass Transfer,

17(10), 1191-1207, 1974.
19. Sheikholeslami M, Mahian O, "Enhancement of PCM solidification using inorganic nanoparticles and an external magnetic field with application in energy storage systems", Journal of cleaner production, 215, 963-977, 2019.
20. Tiari S, Qiu S, Mahdavi M, "Numerical study of finned heat pipe-assisted thermal energy storage system with high temperature phase change material", Energy Conversion and Management, 89, 833-842, 2015.
21. Mahdi JM, Nsofor EC, "Solidification of a PCM with nanoparticles in triplex-tube thermal energy storage system", Applied Thermal Engineering, 108, 596-604, 2016.
22. Vyshak NR, Jilani G, "Numerical analysis of latent heat thermal energy storage system", Energy conversion and management, 48(7), 2161-2168, 2007.
23. Thippeswmay P, Bhaskar A, Mondal S, "An Experimental Study of a LTES with Compact Heat Exchanger Model" In Advances in Energy Research, Vol. 1: Selected Papers from ICAER 2017, 321-329, Singapore: Springer Singapore, 2020.
24. Mosaffa AH, Talati F, Tabrizi HB, Rosen MA, "Analytical modeling of PCM solidification in a shell and tube finned thermal storage for air conditioning systems", Energy and buildings, 49, 356-361, 2012.
25. Krishnamoorthi S, Prabhu L, Kuriakose G, Harikrishnan J, "Air-cooling system based on phase change materials for a vehicle cabin", Materials Today: Proceedings, 45, 5991-5996, 2021.
26. Gürbüz H, Aytaç HE, Hamamcıoğlu E, Akçay H, "The Effect of $Al_2O_3$ Addition on Solidification Process of Phase Change Material: A Case Study on Heating of Automobile Cabin in Cold Climate Conditions", International Journal of Automotive Science and Technology, 6(3), 275-283, 2022.
27. Rubitherm Technologies, "PCM RT-Line.". URL https://www.rubitherm.eu/media/products/datasheets/Techdata_-RT55_EN_09102020.PDF. Accessed January 5, 2023.
28. Gürbüz H, Ateş D, "A numerical study on processes of charge and discharge of latent heat energy storage system using RT27 paraffin wax for exhaust waste heat recovery in a SI engine", International Journal of Automotive Science and Technology, 4 (4), 314-327, 2020.
29. Ateş D, "CFD Analysis of Storage and Re-use by PCM of Exhaust Waste Heat Energy in an Internal Combustion Engine (in Turkish)", Master thesis, Süleyman Demirel University, Graduate-School of Natural and Applied Sciences, Isparta, Turkey, 2019.